**Proceedings of the ASME 2020**
**International Design Engineering Technical Conferences & Computers and Information in Engineering Conference**
**IDETC-CIE 2020**
**August 16-19, St. Louis, MO, USA**

**IDETC-CIE 2020-###**

# RECONSTRUCTION OF GROUND REACTION FORCE DATA USING LYAPUNOV FLOQUET THEORY AND INVARIANT MANIFOLD THEORY.

**Sandesh G. Bhat[1], Thomas G. Sugar[1,2], Sangram Redkar[1]**

[1]Arizona State University, Mesa, Arizona, U.S.A.
[2]ASME Fellow

## ABSTRACT

*Ground Reaction Force (GRF) is an essential gait parameter. GRF analysis provides important information regarding various aspects of gait* [1]–[3]. *GRF has been traditionally measured using bulky force plates within lab environments. There exist portable force sensing units, but their accuracy is wanting. Estimation of GRF has applications in remote wearable systems for rehabilitation, to measure performance in athletes, etc. This article explores a novel method for GRF estimation using the Lyapunov-Floquet (LF) and invariant manifold theory. We assume human gait to be a periodic motion without external forcing. Using time delayed embedding, a reduced order system can be reconstructed from the vertical GRF data. LF theory can be applied to perform system identification via Floquet Transition Matrix and the Lyapunov Exponents. A Conformal Map was generated using the Lyapunov Floquet Transformation that maps the original time periodic system on a linear Single Degree of Freedom (SDoF) oscillator. The response of the oscillator system can be calculated numerically and then remapped back to the original domain to get GRF time evolution. As an example, the GRF data from an optical motion capture system for two subjects was used to construct the reduced order model and system identification. A comparison between the original system and its reduced order approximation showed good correspondence.*

Keyword: Computational Dynamics of Bio-Mechanical and Biological Systems; System Identification; Sensors; Nonlinear Dynamical Systems.

## NOMENCLATURE

| | |
|---|---|
| $x(\,)$ | State space of the original system |
| $\alpha(\,)$ | Linear part of the given system |
| $\epsilon(\,)$ | Combined non-linear part of the given system |
| $M(\,)$ | External forcing on the system |
| $\phi(\,)$ | State Transition Matrix (STM) |
| $\Phi(\,)$ | Floquet Transition Matrix (FTM) |
| $\lambda$ | Lyapunov Exponent |
| $z(\,)$ | State of sapped system |

## 1. INTRODUCTION

Human gait has been a topic of research since 1895 [4] where Fischer et al. studied the biomechanics of human gait under varying conditions. Human gait analysis mainly involves analyzing kinetic, kinematic and electromyographic data. Ground Reaction Force (GRF) is an integral part of the kinetics of human gait. Researchers have utilized the GRF to analyze walking and running gait. [1] and [3] studied the symmetrical nature of the GRF between the left and right leg during walking and running in human beings. Marasović et. al., in their article [2], analyzed normal human gait for 40 participants using their GRF data in order to investigate its different aspects. The methods used to measure GRF data vary widely. In lab environments, instrumented treadmills are preferred cause of their ease of use as seen in [5], [6]. In [7], Paolini et. al. proposed and tested a modified instrumented treadmill with static and dynamic force measurement capabilities in three axes.

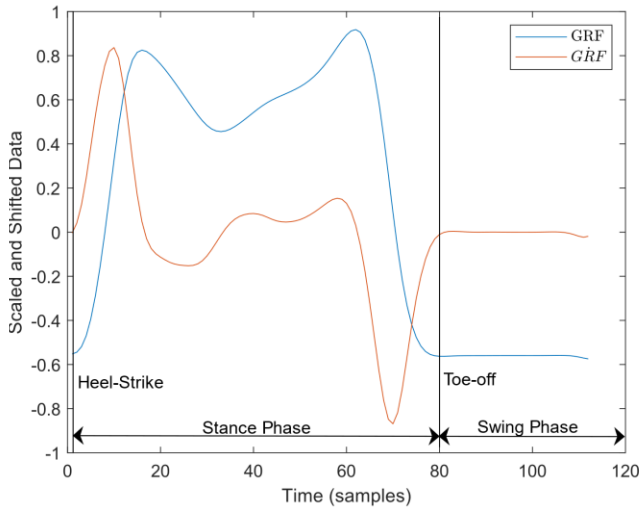


**FIGURE 1**. Data for subject A over one gait cycle, shifted and scaled

Instrumented treadmills have a high accuracy but are bulky and difficult to use outside lab environments. Wireless wearable sensors facilitate portability. Fong et. al. used pressure insoles with 99 sensors to estimate GRF data [8]. They used force plate data to perform regression and fit a model onto the insole output. Wu et. al. used a tactile sensing array to measure the GRF for their robots [9]. Djuric et. al. used a custom-built miniature sensor that used inductive elements to detect GRF [10].

The reason these sensors are not an industry standard in gait analysis is their low accuracy. The sensors on their own could not produce reliable data. As mentioned earlier, [8] used a regression operation to fit their model to the sensor data. Howell et. al. optimized the placement of the sensor in their insole to obtain reliable data [11]. Researchers have used various algorithms in conjunction with their devices to improve accuracy. Hence there is a need for a robust and stable data processing operation that would provide a good approximation of the GRF data. In our article [12], we proposed such an estimation algorithm that used some initial data from the human subject to construct the reduced order model and system identification. In this article, we propose the application of the algorithm in GRF estimation. The algorithm utilized the properties of quasi-periodicity of gait and applied the Lyapunov-Floquet Theory and Invariant Manifold theory to it. Some of the major concepts used in the algorithm are as follows.

## 2. CONCEPTS

### 2.1 Dynamical System Theory in Gait Application:

The human gait system is dynamically complicated to analyze. Researchers have used different ways to approach the problem [13]–[24] while approximating the behavior of the system. Although human gait is not purely periodic, an assumption can be made, and the human gait system, along with the GRF, can be analyzed as a periodic system. Such a periodic system can be represented as

$$\dot{x} = \alpha(t)x + \epsilon(x,t) + M(t),\ x \in \mathbb{R}^n \qquad (1)$$

where $\alpha(t)$ and $\epsilon(x,t)$ are both periodic over $T$ i.e. $\alpha(t) = \alpha(t+T)$ and $\epsilon(x,t) = \epsilon(x,t+T)$. $\epsilon(x,t)$ is the combined nonlinear term of the system. $M(t)$ is the forcing term [24]. The linear form of equation (1) without any forcing term is represented by

$$\dot{x}(t) = \alpha(t)x(t) \qquad (2)$$

We assumed human walking gait was periodic linear system without external forcing and performed further analysis.

### 2.2 Lyapunov-Floquet Theory:

For any nth-order linear periodic system, as in equation (2)

$$\dot{x}(t) = \alpha(t)x(t),\ x \in \mathbb{R}^n \qquad (3)$$

the solution is given by

$$x(t) = \phi(t,t_0)x_0 \qquad (4)$$

where $\phi(t,t_0)$ is the State Transition Matrix (STM) for the given system, valid from time $t_0$ to $t$. Considering $t_0 = 0$,

$$\phi(t,0) \equiv \phi_0(t) \qquad (5)$$

Hence, for $t_0 = 0$ equation (4) becomes,

$$x(t) = \phi_0(t)x_0 \qquad (6)$$

Floquet normal form for the system in equation (6) would be

$$\phi_0(t) = \theta(t)e^{\xi t} \qquad (7)$$

where $\theta(t)$ is a non-singular $n \times n$ periodic matrix with period T and $\xi$ is a $n \times n$ constant matrix. The system is defined as T-periodic. Hence it follows that $\phi_0(t)$ is also periodic over T [15], [16], [24] i.e. $\phi_0(0) = \phi_0(T)$. If the initial conditions are defined as identity (i.e. $x_0 = I_{n\times n}$) then,

$$\phi_0(0)x_0 = x(0) \qquad (8)$$

$$i.e.\ \phi_0(0) = I_{n\times n} \qquad (9)$$

Hence, from equations (7) and (9) it is clear that

$$\phi_0(0) = \theta(0) = I_{n\times n} \qquad (10)$$

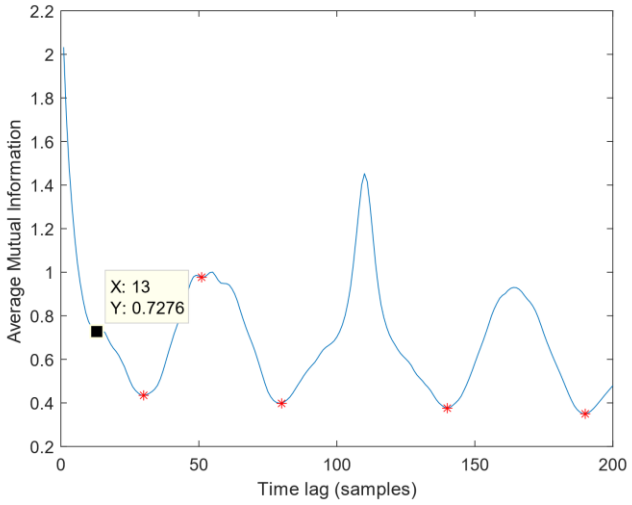


**FIGURE 2**. AVERAGE MUTUAL INFORMATION VS TIME LAG PLOT FOR SUBJECT A BLUE LINE INDICATES THE AMI AND RED ASTERISKS INDICATE THE MINIMA.

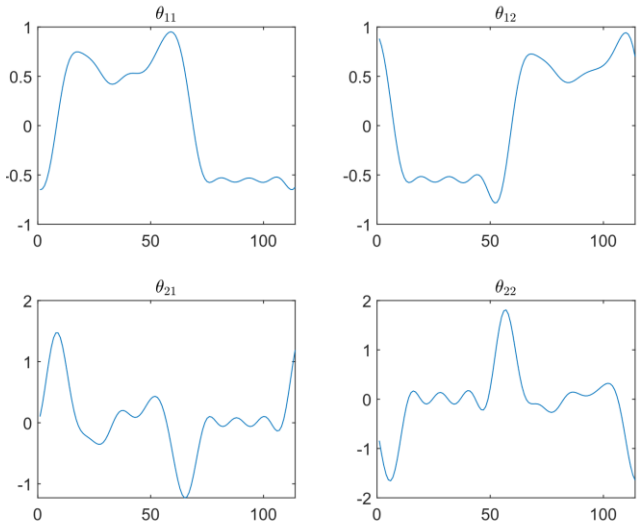


**FIGURE 3**. Elements of the $\theta(t)$ matrix for subject A plotted over one time period ($T$ = *109 samples*)

Since $\theta(t)$ is periodic over T, $\theta(T) = I_{n\times n}$. Hence, from equation (7), $\phi_0(T)$ is a constant.

$$\text{i.e. } \phi_0(T) = e^{\xi T} \tag{11}$$

This representation of the state transition matrix at period T is also known as the Floquet Transition Matrix (FTM). Let the FTM be denoted by $\Phi(T)$ i.e. $\Phi(T) = \phi_0(T) = \mathrm{e}^{\xi T}$. At time $t = T$, equation (4) can represented by $x(T) = \Phi(T)x_0$. Therefore, to calculate the FTM, one can use the values of the state variables at $t = 0$ and $t = T$.

$$i.e. \Phi(T) = x(T)x_0^{-1} \tag{12}$$

The above analysis is true for a continuous system. It could be applied to a discrete time series, but it would be difficult to obtain the original system's dynamical properties using a one-dimensional time series. To analyze a scalar one-dimensional time series, the data needs to be embedded with a suitable time-delay.

### 2.3 Time-Delayed Embedding:

A time series is a projection of the unobserved internal elements of a dynamical system onto the real domain [25]. This projection can be nonlinear and affected by the internal variables of the original system. This might lead to problems in reconstructing the phase space response of the original system. Embedding such a time series is required to reconstruct the original system and its dynamical properties. According to H. Kantz et al. [25] embedding is a mapping operation where a smooth manifold $H$ into $\mathbb{R}^m$ is defined as a map $K$ which is a one-to-one $C^1$ map with a Jacobian $DK(t)$ with full rank everywhere. Taken's time delay embedding theorem [26] reconstructed the phase space using a time delayed time series. The delay vector is defined as $\big(s(x_n), s\big(K(x_n)\big), s\big(KoK(x_n)\big), \dots\big)$ where $x_n$ is the state vector and $K$ is the map represented by $x_{n+1} = K(x_n)$. Let $\tau$ denote the time delay variable. The preferred value of $\tau$ is small. Usually, a large $\tau$ will complicate the reconstruction of the attractor system. It must be noted the underlying mathematics of the system is not affected by the value of $\tau$. An optimum value of $\tau$ cannot be found as there is no proven method to calculate it [25].

There are multiple ways to find the embedding dimension. Principal Component Analysis (PCA) is one of them. PCA is also known as Singular Value Decomposition (SVD). It is a technique to characterize the data into its most important components in the embedding space $\mathbb{R}^m$ [25]. The value of $m$, after a certain value does not affect the underlying properties of the actual system. It must be noted, that a large value of $m$ would increase the computational requirements. Hence the value of $m$ must be selected carefully.

### 2.4 Invariant Manifold:

An Invariant Manifold is a geometric construct that is not affected by the flow of the system. A manifold can be defined as a subset $\mu \subset \mathbb{R}^n$, locally represented as a graph of a smooth function. The manifold is termed invariant if under the effect of a flow $\eta$, for every $x \in \mu$, $\eta_t(x) \in \mu$ for a small $t > 0$. A co-ordinate transformation can be defined representing the local invariant manifold. Let such a transformation of co-ordinate system be described by $\Psi: \Upsilon \to \mathbb{R}^k \times \mathbb{R}^{n-k}$ in the neighborhood $\Upsilon \subset \mathbb{R}^n$ [17]. Let the local co-ordinate system of $\Psi$ be defined as the z domain.

We defined the transformation of our system to a linear system as $f(t) = \theta(t)z(t)$, where $f(t)$ was the original system and $z(t)$ was the transformed linear system. We applied the above defined concepts to the GRF data for walking gait of healthy human subjects. The next section describes the process of data collection and analysis.

## 3. APPLICATION

### 3.1. Data Collection:

We performed normal walking test on two subjects walking on a treadmill (Bertec split-belt instrumented treadmill). Vertical ground reaction force data was collected for 3 minutes at a constant walking speed of 1.2 $ms^{-1}$. The experiments were performed under Arizona State University's Institutional Review Board (STUDY 00009416). The data for the subject's right leg was collected at 1000 Hz but was down-sampled later at 100 Hz and filtered using a low-pass Butterworth filter (cut-off frequency of 10 Hz). The data was down sampled to reduce the processing requirements for the algorithm. The data was divided into individual gait cycles (heel-strike to heel-strike).

### 3.2. Algorithm:

The analysis was performed on MATLAB 2018 A. A derivative was calculated for the GRF data ($\dot{GRF}$). The GRF data along with its derivative formed the response of the original system. Figure 1 shows the GRF and $\dot{GRF}$ data along with the heel-strike and toe-off event markers. The stance and swing phase intervals are also marked in Figure 1. The data was prepared for the algorithm by scaling and shifting the data. It was then chopped at two points and merged to form the system

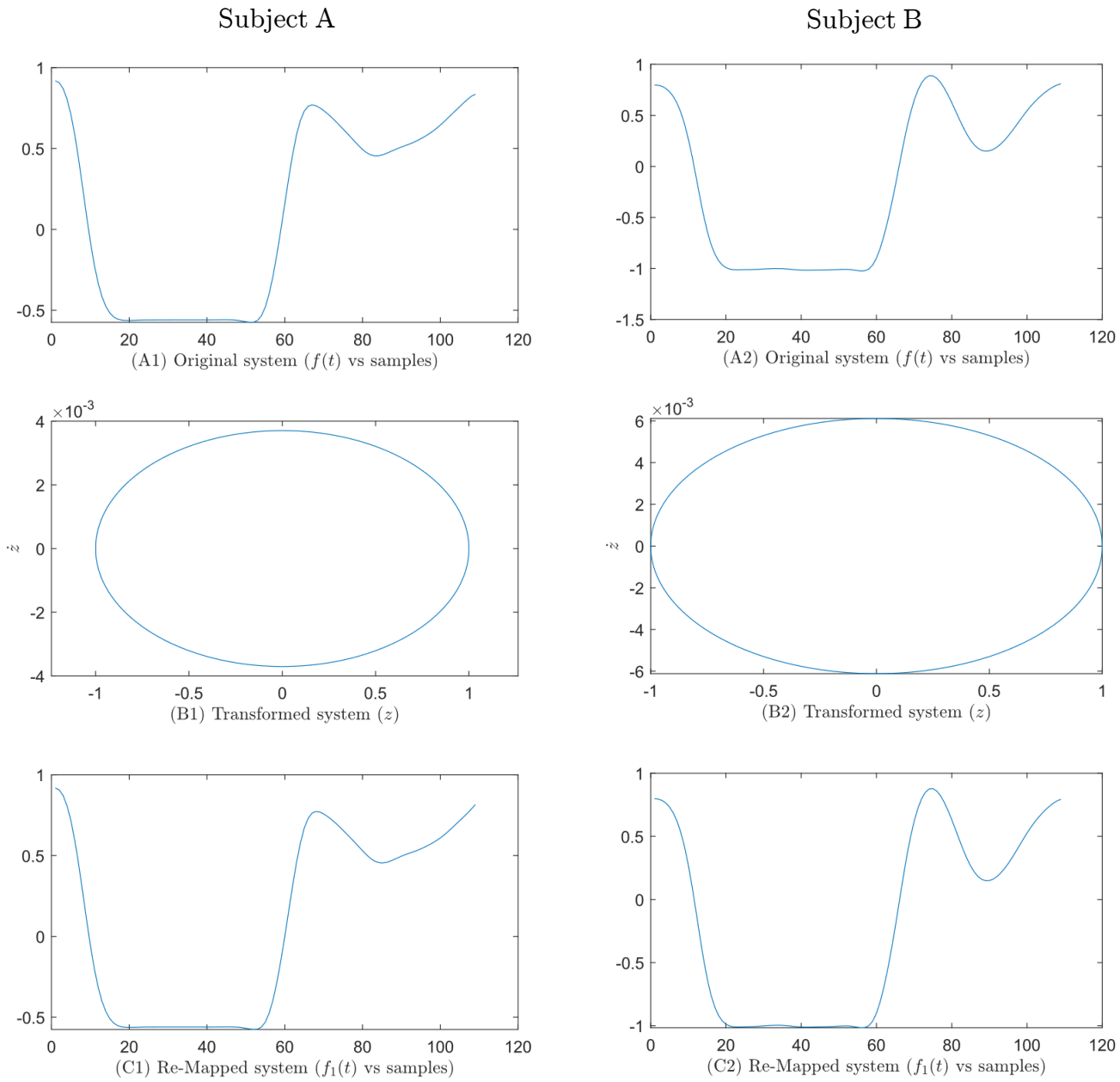


**FIGURE 4.** Transformation of the original system ($f(t)$) (A1, A2) to the linear system ($z(t)$) (B1, B2) and back to the original system domain ($f_1(t)$) (C1, C2) for both the subjects.

$f(t)_{2\times2}$ for any given time $t$. The above operation resulted in the initial condition of the system to be close to zero

$$\text{i.e. } f(0) \approx I_{2\times2} \tag{13}$$

The average mutual information (AMI) was calculated using Leontitsis's MATLAB code [27]. As specified in [25], the first minimum was considered as the time lag ($\tau$) (as seen in Figure 2). The embedding dimension ($m$) required to accurately reconstruct the system dynamics was calculated using the SVD approach. The time-delayed data was layered on top of the original data and the system was reconstructed as detailed in [13] and [16]. The reconstructed system was sensitive to the number of gait cycles considered for the calculation. The goal of the algorithm was to find a reconstructed system that was simply stable (i.e. eigen value close to unity). Hence, the code included a loop to optimize this metric. The eigen value of the FTM was calculated for different numbers of gait cycles and the case with absolute value of the eigen value closest to unity was considered. The FTM was calculated for the reconstructed system as stated in equation (12) for the optimum number of gait cycles. The Exponent Matrix ($\xi$) was the matrix log of the FTM (which was constant for a given system) as derived from equation (11). The eigen value of the $\xi$ matrix was the Floquet Exponent of the system. The real part of the Floquet Exponent is called the Lyapunov Exponent ($\lambda$). The Lyapunov Exponent was used to generate the invariant manifold (i.e. the linear SDoF oscillator). The oscillator had the form

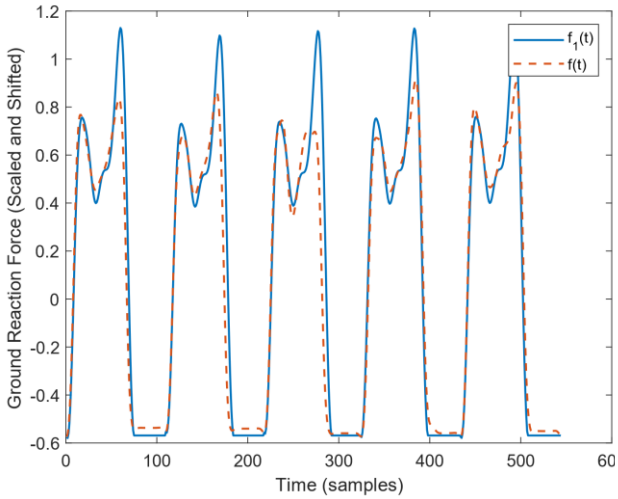


**FIGURE 5**. Comparison between the original system ($f(t)$) and the remapped system ($f_1(t)$) for subject A over five gait cycles.

$$\ddot{z} + \lambda^2 z = 0 \tag{14}$$

The system in the z domain was related to the original system by the relation

$$f(t) = \theta(t)z(t) \tag{15}$$

Hence, the initial condition for the $z(t)$ system was obtained from the expression $z(0) = \theta(0)^{-1} f(0)$. Equation (15) was used to remap the behavior of the $z(t)$ system back to the $f(t)$ domain. The remapped system was termed as $f_1(t)$. The above algorithm was applied to the GRF data from the two subjects. A comparison was drawn to quantify the output of the algorithm.

## 4. RESULT

For the sake of brevity, we will discuss the parameters calculated for only one subject in detail. This subject was classified as subject A. The data collected from the walking tests were discrete (sampled at 100 Hz). Hence, time was expressed in samples. In order to satisfy the condition in equation (13), the data was shifted and scaled as in Figure 1. The average time period (T) for each gait cycle for subject A was calculated to be 109 samples. Time lag was calculated to be 13 samples (first minima as stated in [25]) as seen in Figure 2. The number of gait cycles that led to a stable reconstruction of the original system was 6 gait cycles. Next, the embedding dimension was calculated using the SVD method. The optimum embedding dimension value was calculated to be 24. With this value of $m$, the eigen values of the FTM were close to unity. The initial condition of the $f(t)$ system was close to identity:

$$f(0) = \begin{bmatrix} 0.92 & 0.16 \\ 0.03 & 0.8 \end{bmatrix} \tag{16}$$

The FTM was calculated for the $f(t)$ system for the calculated $m$, $\tau$, and number of gait cycles, and the absolute value of its eigen values were 1.0037. Hence, the system was simply stable. The absolute value of the Lyapunov exponents of the system were 0.0037. The mapped SDoF system was:

$$\ddot{z} + 0.0000137z = 0 \tag{17}$$

All the time series elements of the $\theta(t)$ matrix were fit with a Fourier series to get rid of inconsistencies over multiple gait cycles. The Fourier fit time series in the $\theta(t)$ matrix for subject A over one gait cycle were as seen in Figure 3. The system in equation (17) was reinitialized after every gait cycle. Similar values were calculated for subject B. Figure 4 shows one time period of the original system (Figure 4 A1, A2), the behavior of the $z(t)$ system for the two subjects (Figure 4 B1, B2), and the remapped systems (Figure 4 C1, C2).

The system was remapped using the relationship in equation (15). The reconstruction of the GRF was compared with the original system as seen in Figure 5 and Figure 6. We analyzed the output of the algorithm. They were as discussed below.

## 5. ANALYSIS

Our goal was to use the algorithm presented in [12] to estimate the GRF using just some preliminary data from the user. The algorithm required GRF data for its preliminary calculations. This was considered a training set of data which

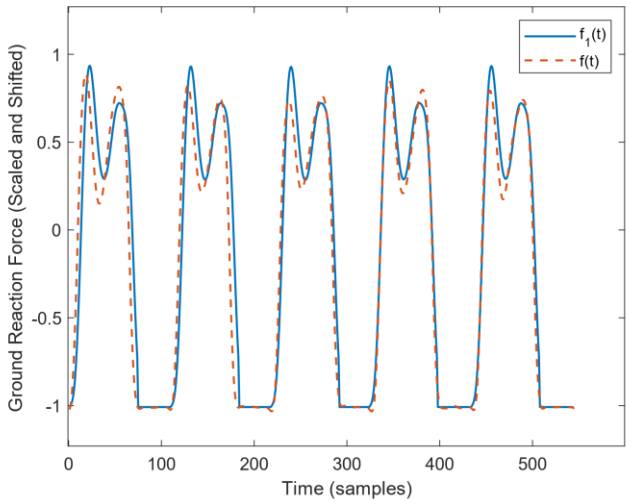


**FIGURE 6.** Comparison between the original system ($f(t)$) and the remapped system ($f_1(t)$) for subject B over five gait cycles.

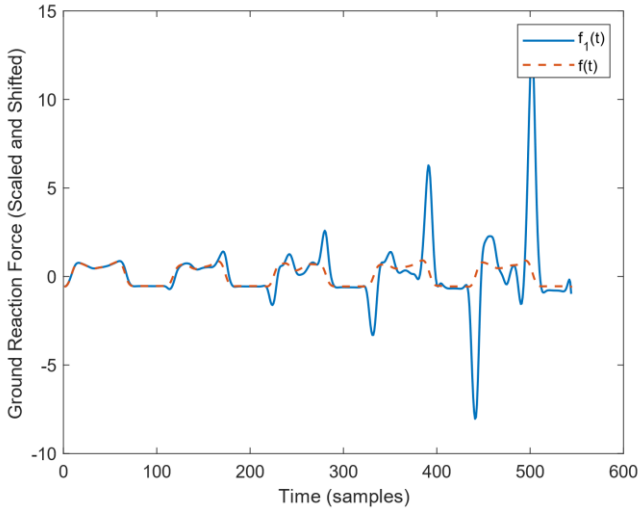


**FIGURE 7.** Reconstructed system ($f_1(t)$) without reinitialization of the $z(t)$ system for subject A.

was used to create a model for reconstructing the GRF data. We used an instrumented treadmill to mitigate any inaccuracy while building our model. After the model was "trained", the algorithm could be applied to an inertial motion capture system with heel-strike detection capabilities. The algorithm was different than machine learning cause of its lack of regression and other statistical analysis tools. But, like machine learning algorithms, the data needed to be scaled and shifted to be used with the algorithm. This introduced additional computational requirements. The results presented in the previous section were calculated post-data collection. The performance of our algorithm in a real-time application will be tested in the future.

As expected from a linear SDoF oscillator, its phase space diagram was an ellipse for both the subjects. The major axis for the $z(t)$ system was considerably larger than the minor axis as evident from the Lyapunov Exponent. The semi-major axis, in both cases, was unity while the semi-minor axis was equal to the absolute value of the Lyapunov exponent of the reconstructed system. It must be noted that a single gait cycle for the original system mapped onto just a minor part of the $z(t)$ system. The time period of the $z(t)$ system was large (169816 samples) and encompassed multiple gait cycles of the original system. But, the $z(t)$ system could not be used for its entire time period.

The re-mapping operation, on its own, did not have a similar behavior as the original system. The $z(t)$ system had to be reinitialized for every gait cycle, from heel-strike to the toe-off event, in order to improve the reconstruction of the GRF after remapping. Hence, only a minor part (approximately 74 samples) of the $z(t)$ system was used after reinitialization. The swing phase, which does not have a GRF, was populated with the value at toe-off until another heel-strike event was detected. Figure 7 shows a comparison between the reconstructed system without reinitialization of the conformal map, and the original system. The response of the system greatly improved after the reinitialization operation (as seen in Figure 5).

Since the system was assumed to be periodic, the time period was constant. This led to a few instances where the original system gait cycle and the remapped system gait cycle did not match (Figure 7). The quasi-periodic behavior of the original system resulted in a varying time period for each gait cycle. Reinitializing the remapped system mitigated some of this irregularity. Providing the algorithm with heel-strike instance data led to a better correlated time series. Hence, if the discussed algorithm were to be applied in a wearable system, the presence of a method to detect heel-strike would be necessary.

The application of this algorithm in a wearable sensing system would lead to an accurate estimation of the GRF. As mentioned earlier, the algorithm will require only a few gait cycles worth of data to be trained. Also, it would be interesting to see the output of the algorithm for human gait at varying speeds. We suspect the Lyapunov Exponents would change dependent on the walking speed (since the time period of gait would decrease). A relationship between the Lyapunov Exponent, the $\theta(t)$ matrix, and the subject's physical parameters (height, weight, leg length, stride length, etc.) would help in designing a general gait model. Such a model could be utilized to obtain GRF curves without the need to train the model for a particular subject. These wearable system would need a way to detect heel-strike events similar to the ones detailed in [29], [30].

## 6. CONCLUSION

In this article, we applied the invariant manifold approach to construct reduced order model for the GRF data of healthy human walking gait. The reconstruction of GRF data using the algorithm was comparable to the data measured using a force plate. One the reduced order oscillator model was constructed; it can be numerically integrated to find GRF evolution w.r.t time. This calculated GRF shoed the same topology of the experimentally obtained GRF. Thus, this approach may be used to estimate the GRF without using a force plate. The next steps would be to apply the algorithm to walking gait of varying speed and analyze the dynamical system properties for different speeds as well as different body weights.


## AKNOWLEDGEMENTS

We would like to thank Arizona State University for supporting this venture.


## REFERENCES


[1] J. Hamill, B. T. Bates, and K. M. Knutzen, "Ground reaction force symmetry during walking and running," *Res. Q. Exerc. Sport*, vol. 55, no. 3, pp. 289–293, 1984.

[2] T. Marasović, M. Cecić, and V. Zanchi, "Analysis and interpretation of ground reaction forces in normal gait," *WSEAS Trans. Syst.*, vol. 8, no. 9, pp. 1105–1114, 2009.

[3] G. Giakas and V. Baltzopoulos, "Time and frequency domain analysis of ground reaction forces during walking: an investigation of variability and symmetry," *Gait Posture*, vol. 5, no. 3, pp. 189–197, 1997.

[4] O. Fischer and W. Braune, *Der Gang des Menschen: Versuche am unbelasteten und belasteten Menschen*. Hirzel, 1895.

[5] P. O. Riley, G. Paolini, U. Della Croce, K. W. Paylo, and D. C. Kerrigan, "A kinematic and kinetic comparison of overground and treadmill walking in healthy subjects," *Gait Posture*, vol. 26, no. 1, pp. 17–24, 2007.

[6] P. O. Riley, J. Dicharry, J. Franz, U. Della Croce, R. P. Wilder, and D. C. Kerrigan, "A kinematics and kinetic comparison of overground and treadmill running," *Med. Sci. Sport. Exerc.*, vol. 40, no. 6, pp. 1093–1100, 2008.

[7] G. Paolini, U. Della Croce, P. O. Riley, F. K. Newton, and D. C. Kerrigan, "Testing of a tri-instrumented-treadmill unit for kinetic analysis of locomotion tasks in static and dynamic loading conditions," *Med. Eng. Phys.*, vol. 29, no. 3, pp. 404–411, 2007.

[8] D. T.-P. Fong, Y.-Y. Chan, Y. Hong, P. S.-H. Yung, K.-Y. Fung, and K.-M. Chan, "Estimating the complete ground reaction forces with pressure insoles in walking," *J. Biomech.*, vol. 41, no. 11, pp. 2597–2601, 2008.

[9] X. A. Wu, T. M. Huh, R. Mukherjee, and M. Cutkosky, "Integrated ground reaction force sensing and terrain classification for small legged robots," *IEEE Robot. Autom. Lett.*, vol. 1, no. 2, pp. 1125–1132, 2016.

[10] S. M. Djuric, L. F. Nagy, and M. S. Damnjanovic, "Detection of ground reaction force using a miniaturized inductive displacement sensor," in *Proceedings of 14th International Power Electronics and Motion Control Conference EPE-PEMC 2010*, 2010, pp. T15--7.

[11] A. M. Howell, T. Kobayashi, T. R. Chou, W. Daly, M. Orendurff, and S. J. M. Bamberg, "A laboratory insole for analysis of sensor placement to determine ground reaction force and ankle moment in patients with stroke," in *2012 Annual International Conference of the IEEE Engineering in Medicine and Biology Society*, 2012, pp. 6394–6397.

[12] S. G. Bhat, T. G. Sugar, and S. Redkar, "INVARIANT MANIFOLDS IN HUMAN JOINT ANGLE ANALYSIS DURING WALKING GAIT.," in *Proceedings of the ASME 2020 International Design Engineering Technical Conferences & Computers and Information in Engineering Conference*, 2020. (unpublished; submitted)

[13] R. C. Wagenaar and R. E. A. van Emmerik, "Dynamics of pathological gait," *Hum. Mov. Sci.*, vol. 13, no. 3–4, pp. 441–471, 1994.

[14] M. Anand, J. Seipel, and S. Rietdyk, "A modelling approach to the dynamics of gait initiation," *J. R. Soc. Interface*, vol. 14, no. 128, p. 20170043, 2017.

[15] H. D'Angelo, "Linear time-varying systems: analysis and synthesis," 1970.

[16] C. Chicone, *Ordinary differential equations with applications*, vol. 34. Springer Science & Business Media, 2006.

[17] B. Morris and J. W. Grizzle, "Hybrid invariant manifolds in systems with impulse effects with application to periodic locomotion in bipedal robots," *IEEE Trans. Automat. Contr.*, vol. 54, no. 8, pp. 1751–1764, 2009.

[18] J. Frank, S. Mannor, and D. Precup, "Activity and gait recognition with time-delay embeddings," in *Twenty-Fourth AAAI Conference on Artificial Intelligence*, 2010.

[19] S. Hidaka and T. Fujinami, "Topological similarity of motor coordination in rhythmic movements," in *Proceedings of the Annual Meeting of the Cognitive Science Society*, 2013, vol. 35, no. 35.

[20] M. Perc, "The dynamics of human gait," *Eur. J. Phys.*, vol. 26, no. 3, p. 525, 2005.

[21] D. J. Miller, N. Stergiou, and M. J. Kurz, "An improved surrogate method for detecting the presence of chaos in gait," *J. Biomech.*, vol. 39, no. 15, pp. 2873–2876, 2006.

[22] N. Scafetta, D. Marchi, and B. J. West, "Understanding the complexity of human gait dynamics," *Chaos An Interdiscip. J. Nonlinear Sci.*, vol. 19, no. 2, p. 26108, 2009.

[23] L. M. Decker, F. Cignetti, and N. Stergiou, "Complexity and human gait," *Rev. Andaluza Med. del Deport.*, vol. 3, no. 1, pp. 2–12, 2010.

[24] S. C. Sinha, R. Pandiyan, and J. S. Bibb, "Liapunov-Floquet transformation: Computation and applications to periodic systems," 1996.

[25] H. Kantz and T. Schreiber, *Nonlinear time series analysis*, vol. 7. Cambridge university press, 2004.

[26] F. Takens, "Detecting strange attractors in turbulence," in *Dynamical systems and turbulence, Warwick 1980*, Springer, 1981, pp. 366–381.

[27] A. Leontitsis, "Mutual Average Information." [Online]. Available: https://www.mathworks.com/matlabcentral/fileexchange/880-mutual-average-information.

[28] P. T. Chinimilli, "Human Activity Recognition and Control of Wearable Robots," Arizona State University, 2018.

[29] M. Yuwono, S. W. Su, B. D. Moulton, and H. T. Nguyen, "Unsupervised segmentation of heel-strike IMU data using rapid cluster estimation of wavelet features," in *2013 35th Annual International Conference of the IEEE Engineering in Medicine and Biology Society (EMBC)*, 2013, pp. 953–956.

[30] H. Ju, M. S. Lee, S. Y. Park, J. W. Song, and C. G. Park, "A pedestrian dead-reckoning system that considers the heel-strike and toe-off phases when using a foot-mounted IMU," *Meas. Sci. Technol.*, vol. 27, no. 1, p. 15702, 2015.